

# Excited-State Structure of Oligothiophene Dendrimers: Computational and Experimental Study

Ekaterina Badaeva,<sup>†,‡</sup> Michael R. Harpham,<sup>‡</sup> Ramakrishna Guda,<sup>‡</sup> Özgün Süzer,<sup>‡</sup> Chang-Qi Ma,<sup>||</sup> Peter Bäuerle,<sup>||</sup> Theodore Goodson III,<sup>\*,‡,§</sup> and Sergei Tretiak<sup>\*,‡</sup>

*Department of Chemistry, University of Washington, Seattle, Washington 98195, United States, Department of Chemistry, Applied Physics Program, The University of Michigan, Ann Arbor Michigan 48109, United States, Institute of Organic Chemistry II and Advanced Materials, University of Ulm, 89081, Ulm, Germany, and Theoretical Division, Center for Nonlinear Studies (CNLS), and Center for Integrated Nanotechnologies (CINT), Los Alamos National Laboratory, Los Alamos, New Mexico 87545, United States*

Received: October 7, 2010; Revised Manuscript Received: October 22, 2010

The nature of one and two-photon absorption enhancement in a series of oligothiophene dendrimers, recently proposed for applications in entangled photon sensors and solar cells, has been analyzed using both theory (time dependent density functional theory calculations) and experiment (fluorescence upconversion measurements). The linear absorption spectra exhibit a red shift of the absorption maxima and broadening as a function of dendrimer generations. The two-photon absorption cross sections increase sharply with the number of thiophene units in the dendrimer. The cooperative enhancement in absorption two-photon cross sections is explained by (i) an increase in the excited-state density for larger molecules and (ii) delocalization of the low-lying excited states over extended thiophene chains. Fluorescence anisotropy measurements and examination of the calculated excited-state properties reveal that this delocalization is accompanied by a size-dependent decrease in excited-state symmetries. A substantial red shift of the emission maxima for larger dendrimers is explained through the vibronic planarization of the longest linear  $\alpha$ -thiophene chain for the emitting excited state. For higher generations, the fluorescence quantum yield decreases due to increased nonradiative decay efficiency (e.g., intersystem crossing). The detailed information about the dendrimer 3D structure and excitations provides guidance for further optimizations of dendritic structures for nonlinear optical and opto-electronic applications.

## I. Introduction

Interest in organic dendritic structures grows intensively due to recent advances in their synthesis and characterization techniques and increasing potential for their applications in modern technology.<sup>1–3</sup> Tunability of electronic structure, optical properties, and charge transfer phenomena in these materials with dendrimer size, chemical compositions, and morphology indicated a broad potential of dendritic structures in many different fields ranging from biology to material science. Strong intrachromophore interactions, efficient energy transfer, charge delocalization and migration through the structural design of dendritic architecture are liable for enhanced nonlinear optical properties (especially two-photon absorption (TPA) cross sections) in comparison to their linear counterparts.<sup>2,4–12</sup> Consequently, organic dendrimers have been actively investigated as new artificial light harvesting and solar energy conversion devices,<sup>13–25</sup> as promising materials for organic electronics,<sup>2,26–32</sup> and nonlinear optical applications, such as 3D microfabrication,<sup>33</sup> multiphoton-microscopy,<sup>34</sup> optical power-limiting<sup>35</sup> and sensing,<sup>36,37</sup> and optical signal processing.<sup>38–40</sup> A detailed comprehensive review of properties of organic dendrimers and ap-

plications of those in sensing, catalysis, molecular electronics, photonics, and nanomedicine can be found in ref 3.

Theoretical investigations of the excited-state phenomena provide explicit information about the nature of charge transfer and the degree of excited-state delocalization in dendritic structures. However, owing to their molecular structure complexity and large sizes, ab initio computations of excitations in dendrimers are still rather challenging. Because of increase of the excited-state density with increasing dendrimer generation, the effective few-state models are harder to derive, although some examples have been successfully applied<sup>29,30</sup> to calculate nonlinear responses in branched organic chromophores. Effective excitonic Hamiltonian models are often used to describe charge transfer features in the self-similar planar branched molecules and dendrimers,<sup>41–44</sup> however, they are not readily applicable for the supramolecular calculations of the systems with strong covalent bonding and high geometrical disorder. Approximations to the excitation energies are often done through the ground-state calculations by analyzing the frontier molecular orbitals. For example, ground-state electronic structure and vibrational spectra of the cyclic polythiophenes have been studied by density functional theory (DFT) methods<sup>45</sup> and have revealed that due to high torsional disorder, the HOMO–LUMO gap of these materials decreases with the ring size, and for some species can be smaller than that of linear polythiophenes. However, sophisticated electronic correlations in the dendritic structures sensitive to geometry distortions and interactions

\* To whom correspondence should be addressed. E-mail: (S.T.) serg@lanl.gov; (T.G.) tgoodson@umich.edu.

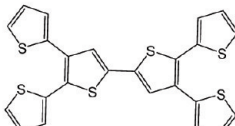
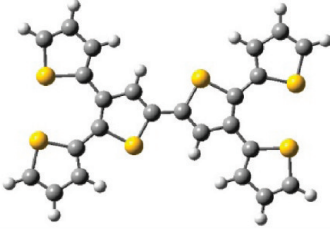
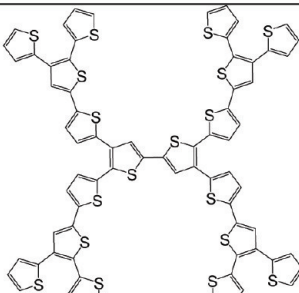
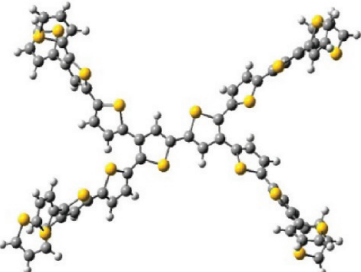
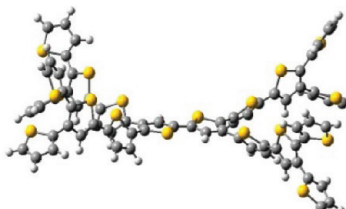
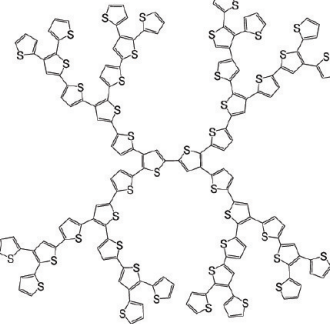
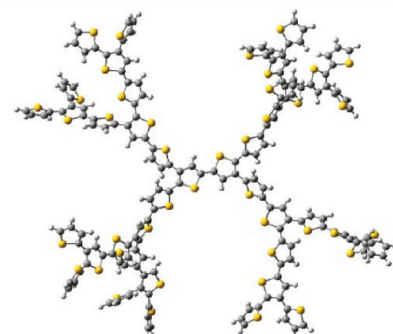
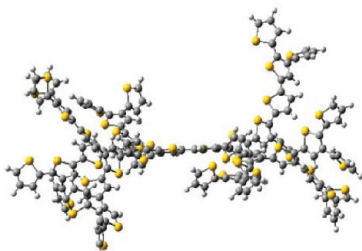
<sup>†</sup> University of Washington.

<sup>‡</sup> Department of Chemistry, The University of Michigan.

<sup>§</sup> Applied Physics Program, The University of Michigan.

<sup>||</sup> University of Ulm.

<sup>¶</sup> Los Alamos National Laboratory.

Name	Chemical Structure	Optimized structure (Front View)	Optimized structure (side view)
S1			
S2			
S3			

**Figure 1.** General scheme and optimized ground-state geometries of the S1–S3 molecules. The next dendrimer generation, S4 (not shown), which has 90 thiophene units, has been synthesized and characterized experimentally as well.<sup>37</sup>

between branches, require more advanced methods for description of linear and, especially, nonlinear spectroscopies of these materials.

Among several organic chromophores utilized for synthesis of dendritic structures, thiophenes or oligothiophenes find a unique place owing to their well-established and versatile chemistry,<sup>1</sup> high stability, easy processing, unique self-assembling properties, charge transport and applications in organic light-emitting diodes,<sup>46,47</sup> field effect transistors,<sup>48,49</sup> chemo- and biosensors,<sup>50</sup> light-harvesting devices and as solar cells.<sup>51</sup> A detailed review of synthesis, properties, and applications of functionalized oligothiophene-based structures can be found in ref 1. Fundamental mechanism behind oligothiophene applications in light harvesting, solar energy conversion, and organic electronics have been intensively investigated in the literature.<sup>52–54</sup> For example, anomalous excitation energy transfer through torsional relaxation in the polythiophene derivative of poly-[3-(2,5-diethylphenyl)thiophene] (PDOPT) has been reported.<sup>55</sup>

Bauerle and co-workers have synthesized<sup>56</sup> space-filling 3D-functionalized oligothiophene dendrimers (Figure 1) for applications such as light harvesting, solar energy conversion, and optoelectronics. Our recent publications<sup>36</sup> have shown the capability of these dendrimeric materials to act as sensors of entangled photons, which allows possible applications in quantum lithography, imaging, and computing applications. Efficient excitation delocalization and excitation energy transfer

are necessary for the organic materials to mimic natural light-harvesting systems and conversion of solar energy, and large electron mobilities are needed in OLED applications. We have observed<sup>36,37</sup> a superlinear increase in TPA cross-section with an increase in dendron and dendrimer generation, which is ascribed to an increasing degree of excitation delocalization with dendrimer generation. As a result, these materials are considered to be suitable building blocks for energy harvesting and NLO applications. Time-resolved measurements on these dendrimers as a function of generation can be used to determine the extent of excitation delocalization and energy transfer processes, which are needed to evaluate their capabilities in optical applications.

In this work, the energy dynamics of these thiophene-based materials are systematically investigated by time-resolved fluorescence methods and time-dependent density functional theory (TD-DFT). Although there are myriad of investigations of ultrafast excited-state deactivation of polythiophenes or oligothiophenes by pump–probe spectroscopy,<sup>52,57,58</sup> limited amount of results are obtained from femtosecond time-resolved fluorescence.<sup>59–61</sup> Kobayashi and co-workers have investigated<sup>61</sup> the chain-length dependence of time-resolved fluorescence of oligothiophenes and have shown that the initial fluorescence anisotropy was around 0.2 to 0.3. Time-resolved fluorescence measurements have been carried out on Si-connected branched thiophenes by Majima and co-workers.<sup>62,63</sup> In a previous work, we have carried out fluorescence upconversion measurements

**TABLE 1: One-Photon Absorption and Emission Properties<sup>a</sup>**

	$E_{\text{exp}}^{\text{abs}, b}$	$E_{\text{exp}}^{\text{em}, b}$	$E_{\text{theor}}^{\text{e}}$	$E_{\text{theor}}^{\text{e'}}$	$E_{\text{theor}}^{\text{em}}$	$\mu_{\text{ge}}$	$\mu_{\text{ge'}}$	$\mu_{\text{c}^*\text{g}}^{\text{fluor}}$	anisotropy	
									$r(0)$	$r(\infty)$
<b>S1</b>	3.25 (382)	2.57 (483)	3.00 (414)	3.97 (313)	2.50 (496)	8.0	4.4	11.4	0.40	0.11
<b>S2</b>	3.23 (384)	2.26 (548)	2.92 (425)	3.25 (382)	1.97 (630)	10.1	6.7	15.0	0.23	0.087
<b>S3</b>	3.20 (387)	2.17 (570)	2.89 (429)	3.06 (405)	1.89 (657)	11.9	7.2	14.4	0.14	0.019
<b>S4</b>	3.19 (389)	2.08 (596)							0.11	0.011

<sup>a</sup> Experimental and calculated vertical transition energies of the lowest,  $E_e$ , eV (nm), and higher energy,  $E_{e'}$ , eV (nm), OPA allowed excited-states (the oscillator strengths for these states are larger than 0.5); energy of the peak of the fluorescence band  $E_{\text{em}}^{\text{exp}}$ , eV (nm); transition dipole moments to the lowest OPA excited state,  $\mu_{\text{ge}}$  (D), and to the higher energy OPA excitation,  $\mu_{\text{ge'}}$  (D); transition dipole moments between the ground and optimized excited state, ( $\mu_{\text{c}^*\text{g}}^{\text{fluor}}$ ) which defines the radiative decay rate; the last two columns provide information about fluorescence anisotropy decay rates,  $r(0)$  and  $r(\infty)$ . <sup>b</sup> Experimental data from ref 37.

on macrocyclic thiophene networks<sup>7</sup> with cavities in nanometer size regime and have shown that the excitation is delocalized over the entire ring. Femtosecond fluorescence decay and anisotropy decay has been utilized by us<sup>2,10,64</sup> and others<sup>60</sup> to probe the phenomenon of excitation delocalization and energy transport in several branched, macromolecular and dendritic architecture NLO materials. In this paper, time-dependent density functional theory (TD-DFT) in combination with quasiparticle formalism for nonlinear optical polarizabilities is performed with the goal of providing further evidence of excitation delocalization and symmetry-breaking. In particular, we estimate the spatial extent and parity of the optical excitations in the dendrimer molecule, observe the photoinduced energy funneling for the higher-lying excited states, and elucidate the mechanisms of excitation dynamics through fast and slow anisotropy decay traces and TD-DFT calculations. We reveal a systematic increase of excited-states delocalization with the size of the dendrimer, which explains the origins of the cooperative enhancement for the nonlinear optical signals.

## II. Materials and Methods

**A. Materials.** The thiophene dendrimers investigated in this work were synthesized by an iterative divergent/convergent method starting from a trimethylsilyl (TMS)-protected branched terthiophene.<sup>56</sup> A solvent of tetrahydrofuran (THF, Sigma-Aldrich, 99.9% purity) was used for thiophene dendrimer liquid samples. Details on synthesis and sample preparation can be found in ref 36. The optical density for the solutions prepared was controlled by concentration. Steady-state absorption experiments were performed using an Agilent 8341 UV/vis spectrometer and fluorescence measurements with a Jobin Yvon - SPEX Fluoromax-2 spectrometer and are reported in detail elsewhere<sup>36,37</sup> and included in Table 1 of the current work. To measure the two-photon absorption cross sections (TPACS,  $\sigma_2$ ), the two-photon excited fluorescence (TPEF) method has been employed. A  $10^{-4}$  M Coumarin 307 solution in methanol was used as the reference material. A mode-locked Ti:Sapphire laser (Spectra-Physics MaiTai HP, 100 fs, 80 MHz) was used to produce an excitation wavelength over the range of 700–850 nm.

**B. Time-Resolved Fluorescence Measurements.** Details of the fluorescence upconversion experiment (Figure 2) have been reported in detail elsewhere.<sup>64</sup> Briefly, the second harmonic of the output from a Ti:Sapphire oscillator (Spectra-Physics Tsunami, 770–830 nm, < 80 fs) is used as the excitation beam, while the residual fundamental passes through a variable delay line. Horizontally polarized fluorescence from the sample is combined with the time-delayed fundamental at a nonlinear BBO crystal to produce a time-resolved fluorescence kinetic trace. Polarization of the excitation beam is controlled by a Berek compensator. The sample is contained in a 1 mm rotating sample cell. Kinetic traces were obtained using 6.25, 62.5, and

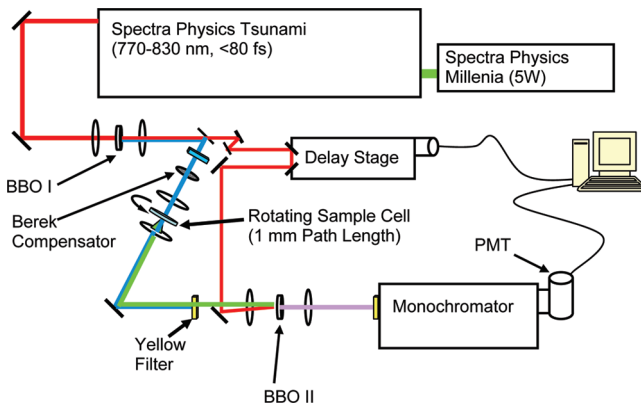


**Figure 2.** Depiction of the fluorescence upconversion experiment (CDP systems FOG-1000).

625 fs steps, corresponding to short, medium, and long time scans. The instrument response function (IRF) was measured using the Raman scattering of water. From a Gaussian fit of the Raman scattering, a full-width half-maximum of 231 fs was obtained. Subsequent fits of the time-resolved fluorescence data did not constrain the IRF, however, the FWHM were all found to be within error ( $\pm 10$  fs) of this value.

Parallel ( $I_{\text{par}}$ ) and perpendicular ( $I_{\text{per}}$ ) decay traces were collected at the fluorescence maxima of the respective dendrimers, as well as at wavelengths 20 nm shorter and longer than the maximum. From these traces, the anisotropy,  $R(t)$ , is calculated from the equation

$$R(t) = \frac{I_{\text{par}}(t) - GI_{\text{per}}(t)}{I_{\text{par}}(t) + 2GI_{\text{per}}(t)}$$

where the  $G$  factor, which accounts for difference in sensitivity of the instrumentation to parallel and perpendicular polarization, was determined to be 0.95.

**C. Quantum Chemistry Calculations.** Adiabatic TD-DFT<sup>65,66</sup> in the Kohn–Sham (KS) form is currently the method of choice for calculating the excited-state structure of large organic molecules.<sup>67,68</sup> TD-DFT extensions for the calculations of molecular nonlinear optical properties have been suggested based on the residues of the quadratic response functions for TPA<sup>69</sup> and on the quasiparticle formalism of the TD-KS equations for arbitrary frequency-dependent nonlinear optical polarizabilities.<sup>69–71</sup> Subsequently, the latter approach was applied to calculate one photon absorption (OPA) and TPA properties of several families of donor/acceptor substituted conjugated organic dyes and branched structures.<sup>28,72–77</sup> Excellent quantitative performance of TD-DFT based on hybrid functionals have been shown for both OPA and TPA responses.

In this study, linear and two-photon absorption spectra of a series of oligothiophene dendrimers, shown in Figure 1, have been modeled with the method described above.<sup>71,72,78</sup> Ground-state geometry optimizations have been performed at the Hartree–Fock (HF) level of theory. 6-31G basis set was used for all calculations. According to our previous studies, this level of theory is sufficiently accurate to describe the geometry of the smaller organic chromophores and large branched structures acceptably well.<sup>72,73,75</sup> The excited-state electronic structure of all molecules was calculated with the TD-DFT formalism implemented in the Gaussian 03 and Gaussian 09 program suites.<sup>79</sup> A total of 20, 40, and 60 excited states, respectively, for **S1**, **S2**, and **S3** were considered to calculate OPA and TPA responses based on the Gaussian output and utilizing the modified collective electronic oscillator (CEO) code.<sup>71,78</sup> Inhomogeneous line broadening parameter for all absorption spectra calculations has been fixed to  $\Gamma = 0.17$  eV for all chromophores based on a typical line width of respective experimental spectra.<sup>31</sup> A detailed description of the computational methodology used for this study can be found in refs 72 and 73. The emission wavelengths and oscillator strengths have been calculated with the TD-B3LYP method following the TD-HF excited-state optimization. Thus, we use HF and TD-HF methods to optimize ground- and excited-state geometries, respectively, and TD-B3LYP technique to calculate excited-state manifolds and analyze the resulting optical responses. This combination is a practical approach to bypass possible problem with description of charge-transfer excitations in TD-DFT, which worked well previously for a variety of molecular systems.<sup>28,31,77</sup> It is well established that TD-DFT calculations based on GGA and hybrid (with small fraction of orbital exchange) functionals frequently result in the appearance of unphysical charge-transfer states in large conjugated molecules with delocalized wave functions. Particularly, unexpected surprises may happen in the course of excited-state geometry optimizations (e.g., ref 80). Finally to understand the nature of excited states involved in the linear and nonlinear absorption processes, natural transition orbital (NTO) analysis has been performed.<sup>81</sup> This approach provides the most compact representation of the electronic transitions on terms of an expansion into single particle orbitals by diagonalizing the transition density matrix associated with each excitation. Figures showing natural transition orbitals were built using Gaussview software.

### III. Results and Discussion

**A. Ground-State Geometry.** The chemical structures and optimized ground-state geometries of the molecules **S1**–**S3** examined in this work are shown in Figure 1. The first generation of the thiophene oligomers (**S1**) is substantially planar. With increasing number of thiophene units, the molecule becomes more 3D-like forming bulky substructure with substantial conformational disorder. The bithiophene core of the larger dendrimers maintains configuration close to planar, with the 7° distortion between the thiophene rings. The side chains are turned by 51 and 55° from the central thiophene moiety in **S2** and **S3**, respectively. The average distortion angle in the side thiophene-chains is 38° for both **S2** and **S3**.

**B. One-Photon Absorption (OPA).** The calculated and experimental one-photon absorption and emission spectra for the molecules **S1**–**S3** are shown in Figure 3 and characteristic OPA properties (energies and transition dipoles) are summarized in Table 1. The next generation of the dendrimer, **S4**, consisting of 90 thiophene units, has been synthesized and characterized experimentally but has not been studied theoretically due to high computational cost. Both experimental and calculated absor-

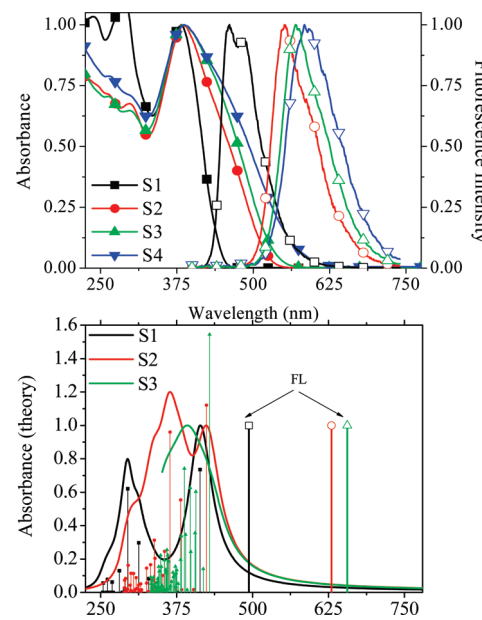


**Figure 3.** (Top) Experimental absorption and fluorescence spectra for dendrimers **S1**–**S4**, adapted from ref 36. (Bottom) Calculated one-photon absorption spectra of molecules **S1**–**S3**. Absolute values of the calculated oscillator strengths are shown in the lower panel as vertical lines. Calculated emission wavelengths (FL, with normalized intensities) are shown as single peaks of the corresponding color and marker: **S1** (dark squares), **S2** (red circles), and **S3** (green triangles).

bance spectra in Figure 3 have two bands in the visible (around 3.2 eV) and near-UV energy regions. Increasing size of the dendrimer leads to a characteristic slight red shift of the lowest absorption peak which is very well reproduced by our computational method. We also observe broadening on the red edge of the low energy absorption band, a result that matches that previously observed in the thiophene dendrons<sup>37</sup> and in a series of the functionalized thiophene-based dendritic structures.<sup>1</sup> The broadening of the red edge of the peak has previously been attributed<sup>37</sup> to absorption by linear chains of  $\alpha$ -thiophene units. Increasing chain length leads to a red shift of the absorption wavelengths, subsequently, the overall spectrum is a linear combination of these various absorptions of segments.

While calculated absorption trends generally agree well with the experimental observations, the absolute values of the theoretical transition frequencies are systematically underestimated by theory. Indeed, our calculations do not account for the solvent effects and a variety of the structural conformations that become possible for larger dendrimers at room temperature. Moreover, the absolute values of TD-DFT transition energies strongly depend on the amount of the Hartree–Fock exchange added to the DFT functional.<sup>80</sup> An increase of the orbital exchange fraction would lead to the blue shift in the calculated excitation energies.

The natural transition orbitals (NTOs)<sup>81</sup> of the brightest OPA-active excited states shown in Figures 4–6 reveal the excited-state nature and support experimental assignments. The lowest OPA-active excited state can be characterized as  $\pi$ – $\pi^*$  transition in the longest linear  $\alpha$ -thiophene chain with some delocalization over the rest of the molecule. A red shift of the absorption maxima is caused by stabilization of these excited states due to elongation of the conjugation length, an effect that is well-known for many conjugated chromophores and polymers,<sup>31</sup> in particular, for thiophene oligomers. Elongation of the absorbing unit causes an increase in the ground-to-excited-state transition dipole moment ( $\mu_{ge}$ ) (see Table 1), which results in an increase of the

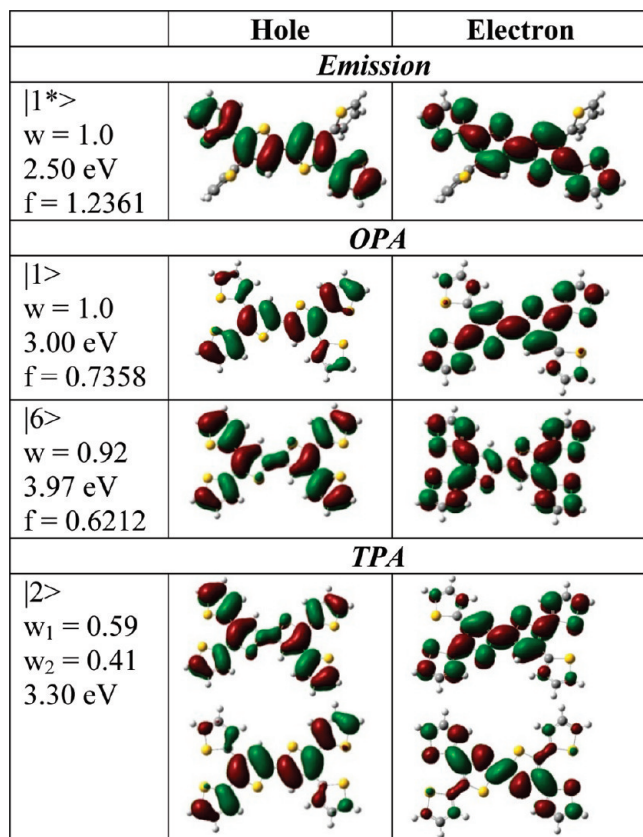


**Figure 4.** Natural transition orbitals describing the lowest optimized excited state (emission), bright OPA states  $e$  and  $e'$ , and the brightest TPA state  $E$  for **S1** molecule. The numbers in the left column indicate the corresponding excited-state number, fraction of the NTO pair contribution into the given electronic excitation,  $w$ , excitation energy in eV, and oscillator strength for the OPA excitations. In the case when the NTO fraction is less than 0.7, two NTO pairs are plotted.

oscillator strength for the lowest OPA transitions (vertical lines in the plot in Figure 3b). As size of the dendrimer grows, the torsional disorder in the molecular structure prevents further delocalization of the excitation, which leads to a saturation of excitation energy value. Thus, no excited state is delocalized on a linear chain with more than 8–9 thiophene units. This result agrees well with the previous studies on linear oligothiophene chains, which show saturation of the linear and nonlinear absorption cross sections as well, as the band gap convergence for 8–9 unit long oligothiophenes.<sup>82</sup>

The transition frequencies for the second (near-UV) absorption band are more size-dependent and vary from 3.96 eV for **S1** to 3.07 eV for **S3**. The brightest peaks in this band correspond to the states mostly localized at periphery of the dendrimer. Besides the delocalized nature of the low-lying excited states, the spectral broadening and increase in absorption intensity is caused by a sharp increase in density of the excited states (DOES) with the dendrimer generation. Since the total absorption spectrum is roughly a linear combination of all possible absorption features, an increase in the amount of optically allowed excited states will lead to an additive increase of the absorption cross-section. The DOES is shown in Figure 3 by the vertical lines. NTOs in Figures 5 (**S2**) and 6 (**S3**) illustrate some examples of the optically active excited states with some charge transfer character from the side dendrimer branches to a central unit (for example, state  $|4>$  for **S2**). Electronic transitions within the shorter dendrimer branches as well as the interbranch charge transfer also contribute to the

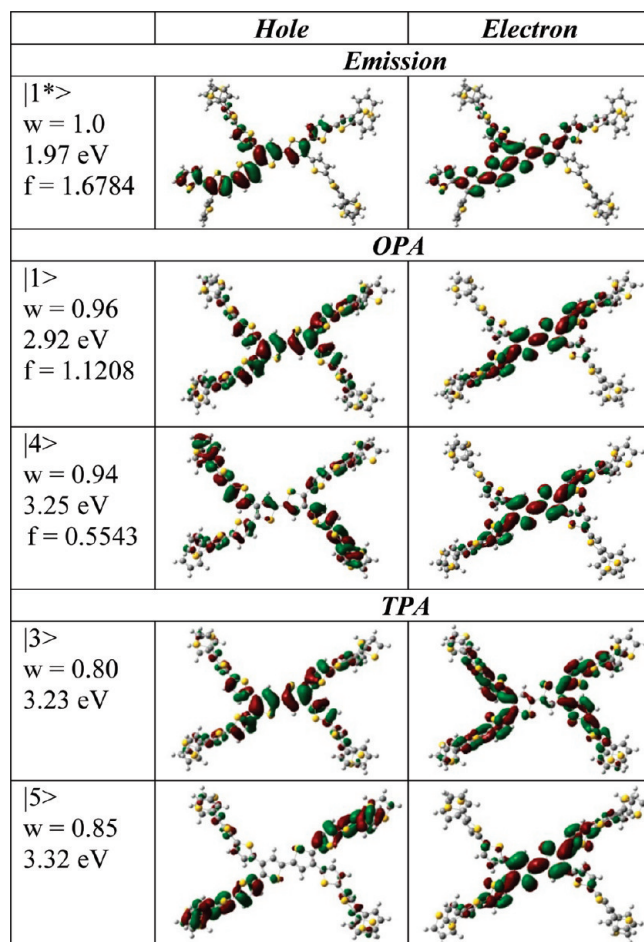


**Figure 5.** Natural transition orbitals describing the lowest optimized excited state (emission), bright OPA ( $e$  and  $e'$ ) and TPA ( $E$  and  $E'$ ) states for **S2** molecule. The numbers in the left column indicate the corresponding excited state, fraction of the NTO pair contribution into the given electronic excitation,  $w$ , excitation energy in eV, and oscillator strength for the OPA excitations.

excited-state density, but they generally appear with smaller oscillator strength. Our calculations do not reproduce well the observed band-broadening as well as the second band maxima positions for larger dendrimers. These features arise from the conformational disorder in larger structures, present at room temperature, which we are currently unable to address computationally. We believe that this information is a clue to interpretation of the spectra for larger molecules.

**C. Fluorescence and Photoinduced Dynamics.** Previously, conventional and time-resolved fluorescence measurements have been performed<sup>37</sup> to understand photoinduced dynamics and vibronic excited-state relaxation. Here we will review the fluorescence experimental findings and relate them to the theoretical data. Experimental and calculated emission maxima are compared in Figure 3. A distinct red shift with increasing dendrimer generation have been experimentally attributed to emission from the longest  $\alpha$ -thiophene chain. Previous experiments on thiophene dendrons have also shown this behavior. The trends in the vertical emission frequencies obtained from TD-DFT calculations are shown in Figure 3b and summarized in Table 1. NTOs for the optimized first excited state for **S1–S3** dendrimers are shown in Figures 4–6, respectively. Optimization of the lowest singlet excited-state geometry indeed leads to planarization of one of the  $\alpha$ -thiophene chains, which is typically accompanied by increased distortions in the rest of the molecule. Such torsional relaxation causes stabilization of

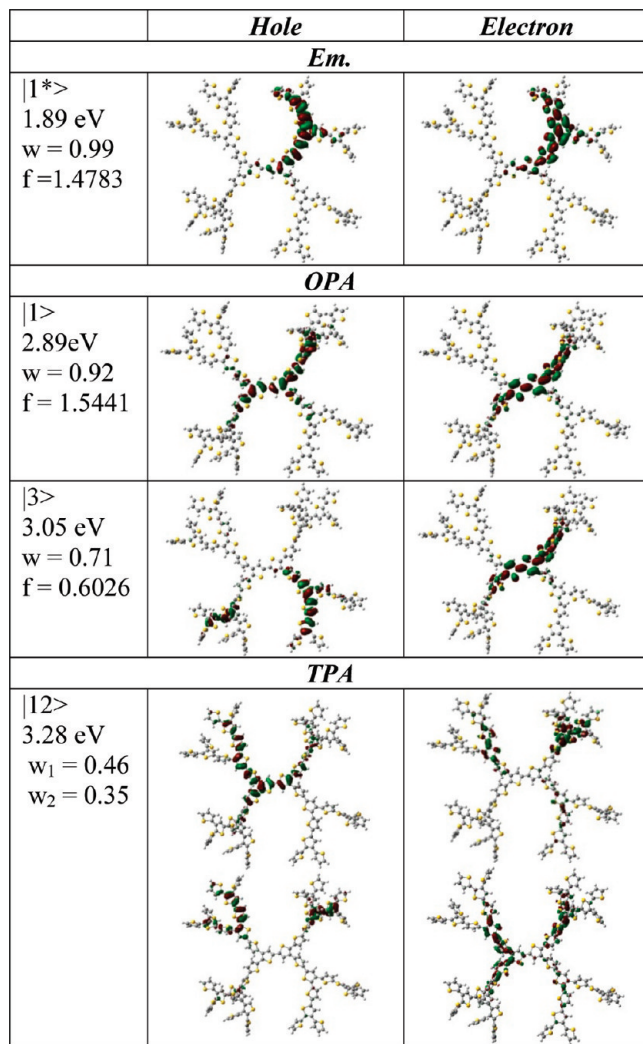


**Figure 6.** Natural transition orbitals describing the lowest optimized excited state (emission), bright OPA states  $e$  and  $e'$ , and one of the allowed TPA states,  $E$  for **S3** dendrimer. The numbers in the left column indicate the excited-state number, fraction of the NTO pair contribution into the given electronic excitation,  $w$ , excitation energy in eV, and oscillator strength for the OPA excitations. In case when the NTO fraction is less than 0.7, two NTO pairs are plotted.

the lowest (emitting) excited state, as has been observed in the linear polythiophenes and other conjugated polymers,<sup>52–54</sup> and can facilitate ultrafast excitation energy transfer to the lowest excited state.<sup>55</sup> The calculated Stokes shifts for the thiophene dendrimers grow with dendrimer size being in a perfect agreement with experimental data, but tend to saturate for higher generations (0.5, 0.95, and 1.00 eV compared to experimental 0.68, 0.97, and 1.03 for **S1**, **S2**, and **S3** molecules, respectively). An increase in the Stokes shift comes from the fact that planarization of the emitting unit leads to a more effective excited-state energy stabilization compared to the distorted  $\alpha$ -thiophene chain.

The observed elongation and planarization of the emitting  $\alpha$ -thiophene chain results in an increase of the excited-to-ground-state transition dipole moment ( $\mu_{eg}^*$ ). Remarkably, for the **S1** transition dipole moment at the excited-state geometry grows by a factor of 2 compared to its value at the ground-state geometry. However, such increase in the transition dipole moment saturates when the size of excitation reaches 7–8 thiophene units. Therefore, the relative increase in the transition dipole moment due to conformational relaxation decreases for

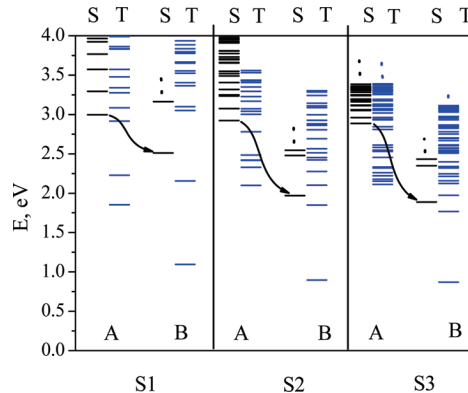


**Figure 7.** Singlet (S) and triplet (T) excited state energies of **S1**–**S3** dendrimers calculated for the ground-state (A) and excited-state (B) optimized geometries. Arrows schematically represent vibronic relaxation for the lowest excited state. Only a few lowest excitations are shown.

higher dendrimer generations. Despite the decrease in the transition frequency, the enhanced transition dipole moment for the emitting state should potentially lead to faster radiative decay rates. However, experimental data shows a decrease in the fluorescence quantum yield for larger dendrimers. This trend may be caused by a concomitant increase in the nonradiative decay rate due to internal conversion to nonemissive singlet states<sup>83</sup> or intersystem crossing to the triplet state manifold. In particular, the effective intersystem crossing in linear  $\alpha$ -oligo-thiophenes has been discussed in earlier studies<sup>84–86</sup> and recently was found to be an effective nonradiative relaxation pathway for the macrocyclic thiophene-derivatives.<sup>7</sup> In our case, such a scenario is further justified by the fact that for larger dendrimers, the vibrational excited-state conformational relaxation requires more time due to the increased length of the  $\alpha$ -thiophene chain. To check this hypothesis, a triplet-state analysis have been performed for all dendrimers. Figure 7 illustrates the excited-state diagram for the manifold of singlet and triplet excited states for the initial ground-state geometry (A) and relaxed excited-state geometry (B). The calculations clearly show that the density of triplet states in the vicinity of the lowest singlet excited state grows with dendrimer generation. Moreover, as is clearly seen from the excitation scheme in Figure 7, the number of triplet states that intersect the potential energy surface for the lowest singlet excited-state relaxation (schematically shown with the arrows) dramatically increases with the size of thiophene molecule. Since the intersystem crossing depends on the overlap between the vibrational wavepackets of the singlet and triplet excitations as well as the value of spin–orbit coupling, the probability of singlet–triplet transition (and nonradiative decay rate) should significantly grow with dendrimer size.

Theoretical findings about excited-state delocalization and relaxation stand along with the time-resolved fluorescence anisotropy (upconversion) measurements, which are summarized in Figures 8–9. The short-time decay of **S3** along with the instrumental response function (IRF) is shown in Figure 8. Short- and long-time anisotropy decay traces are plotted in Figure 9a,b, respectively. For the **S1** dendrimer, a fast decay on the order of 500 fs is observed, but this does not significantly decrease the anisotropy of the system; a long time component on the ~50 ps time scale provides the main contribution to the decay. In the cases of **S2**, **S3**, and **S4** dendrimers, a decay on approximately the same time scale as the instrument response function provides a substantial contribution to the overall anisotropy decay.

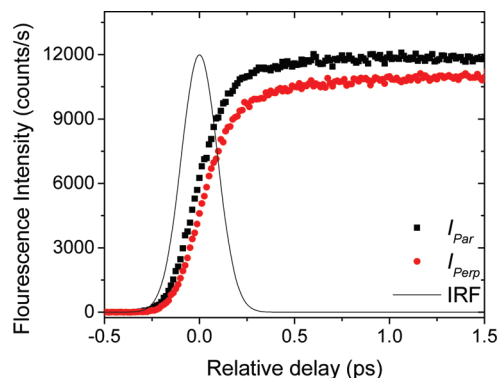


**Figure 8.** Short-time scale fluorescence kinetics of the thiophene dendrimer **S3** after excitation with 400 nm light. Collection wavelength corresponded to fluorescence at 570 nm, which is the one-photon fluorescence maximum.

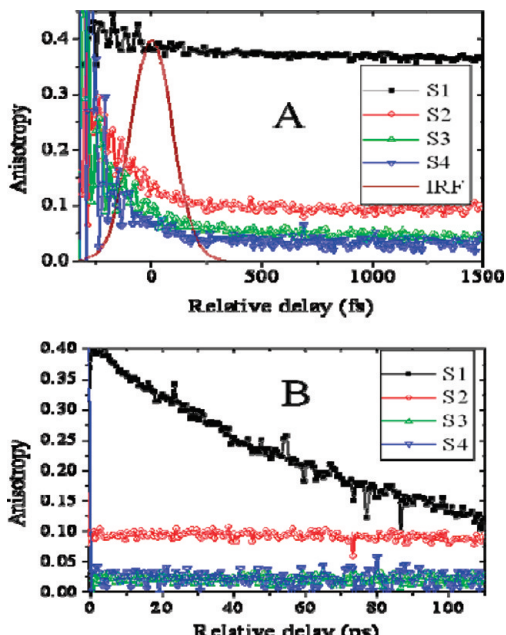


**Figure 9.** (A) Short-time anisotropy decay traces for the various dendrimer generations. (B) Long-time anisotropy decay traces for the various dendrimer generations. Data plotted was collected at the wavelength corresponding to the respective fluorescence maximum of the dendrimer.

The fast decay component can be associated with the strong intramolecular interactions arising from the formation of a delocalized excited state in which the region of delocalization is significantly larger than an individual thiophene unit. This decay component is found to become increasingly faster for the higher dendrimer generation as a result of the increased delocalization present in the larger dendrimers. It is seen (Table 1) that the residual anisotropy decreases with increasing dendrimer generation, suggesting that the excitation delocalization, and hence, transition dipole moment is increasing with dendrimer generation, which is reflected in the enhanced absorption cross-section observed in the larger dendrimers. This trend is strongly supported by the NTO plots (Figures 4–6) and by the data in Table 1, where  $\mu_{ge}$  grows from 8 to 12 D when generation changes from **S1** to **S3**.

**D. Two-Photon Absorption.** Experimental and calculated two-photon absorption spectra for dendrimers **S1–S4** in a range of 700–850 nm are shown in Figure 10. TPA cross sections (TPACS) and excitation energies are summarized in Table 2. Two TPA bands are observed on the calculated spectra. The

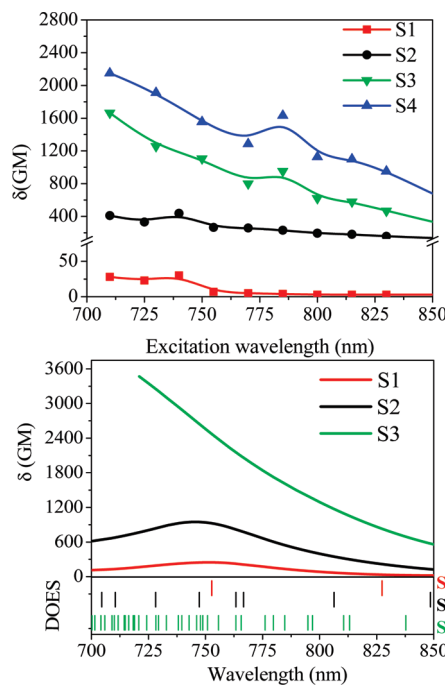


**Figure 10.** Experimental (top panel) and calculated (bottom panel) two-photon absorption spectra for thiophene dendrimers **S1–S4** (adapted from ref 36) (**S1–S3** for the calculations) in the energy region from 700 to 850 nm (1.46–1.77 eV). The lowest plot shows the calculated density of excited states (DOES) that dramatically increases for higher dendrimer generations. Calculated spectra use a line broadening parameter of 0.17 eV consistent with experimental spectra.

**TABLE 2: Two-Photon Absorption Properties<sup>a</sup>**

material	$\sigma_E^{\text{theor}}$	$\sigma_E^{\text{exp}}$	$E_E^{\text{theor}}$	$\sigma_E^{\text{theor}}$
	at 748 nm, GM	at 800 nm, GM	eV (nm)	GM
<b>S1</b>	247	6	1.97 (630)	180
<b>S2</b>	947	230	2.07 (600)	1230
<b>S3</b>	2657	620		
<b>S4</b>		1130		

<sup>a</sup> Experimental and calculated TPA cross sections at the first ( $\sigma_E^{\text{exp}}$ ,  $\sigma_E^{\text{theor}}$ ) absorption maxima (observed at ~800 nm experimentally and ~748 nm by the calculation); calculated transition energies ( $E_E^{\text{theor}}$ ) and TPA cross sections ( $\sigma_E^{\text{theor}}$ ) of the second TPA maximum,  $E_E^{\text{theor}}$ . Steady-state and two-photon absorption cross sections were measured previously and discussed in refs 36 and 37.

lowest band lies in the region between 700 and 850 nm, and a second TPA peak (not shown) is observed in the calculated spectra for compounds **S1** and **S2** at 630 nm (1.97 eV) and 600 nm (2.07 eV), respectively.

The distinct feature of all TPA spectra is substantial increase of the TPACS in a wide energy region for larger dendrimers. The TPA spectra are very broad and do not have well-defined maxima. For example, the TPACS increase from approximately 6 GM for **S1** to 1120 GM for **S4** at 800 nm excitation. Comparing the thiophene dendrimers in this work to nitrogen-centered and plain phenylacetylene dendrimers previously reported,<sup>7,87</sup> the thiophene dendrimer is found to yield a larger TPA cross-section than the phenylacetylene dendrimer does for a given dendrimer generation. Recently, thiophene macrocycles have been reported<sup>7</sup> to have TPA cross sections of  $10^4$ – $10^5$  GM with TPA cross sections per thiophene group of  $10^2$ – $10^3$  GM. The thiophene dendrimers reported here are found to have a smaller TPA cross-section per subgroup compared to the macrocycles. However, the dendrimer architecture may have

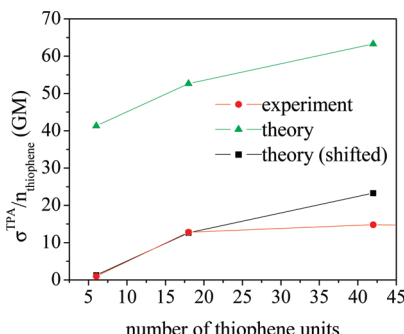


**Figure 11.** Calculated and experimental TPA cross sections normalized by a number of thiophene units in the dendrimer plotted against the number of thiophene units. Theoretical results show a very good agreement with the experimental data, although, the TPA cross-section absolute values are overestimated by the theory. For the eye-guidance, the black curve shows theoretical data with all TPA values shifted down by a constant  $C = 40$  GM. Experimental results shown here have been reported in ref 37. The normalized experimental TPA cross-section value for **S4** dendrimer is  $\sim 13.3$  GM (not shown here).

greater potential in energy transport applications due to the ability of branch-core systems to funnel energy. Theoretical results provide the TPACS for the lower TPA allowed excited states at around 3.3 eV (which would correspond to the excitation energy of  $\sim 750$  nm) growing from 247 GM in **S1** to 2657 GM in **S3**. Although the calculated TPACSs are overestimated relative to experiment, the trends are well-reproduced. The discrepancies in the absolute cross-section values can arise from the underestimated solvent effects, local field factor,<sup>31</sup> and geometry deformations at the room temperature.

To analyze the two-photon absorbance growth with the dendrimer generation, Figure 11 shows the variation of the TPACS at 1.66 eV (absorption maximum) normalized per number of thiophene units against the dendrimer size, compared to the respective experimental values at 1.57 eV (800 nm). The absolute values of the calculated cross sections and the values uniformly shifted by 40 GM are included to trace the agreement between experimental and theoretical data. While the overall TPACS of the material increases with dendrimer generation, the TPACS per thiophene unit saturate for **S3–S4** in experiment and converges to approximately 13 GM/thiophene unit value. In the calculations, we still observe a weak increase of the TPACS per thiophene unit when going from **S2** to **S3** (Figure 11), since in our modeling we do not account for additional disorder effects arising from the solvent dynamics at room temperature in experimental conditions. Thus, the cooperative enhancement in the material becomes less effective as the number of thiophene groups increases.

NTOs for the selected excited states contributing to the TPA spectra (Figures 4–6) show delocalized character of the electron and/or hole orbitals and a more pronounced charge-transfer character, as compared to the OPA excited states. The lowest TPA allowed excited state in **S1** involves transition of an electron from the peripheral branches to the core of the dendrimer. The excited-state parity selection rules (even parity  $\pi-\pi^*$  transitions for the TPA vs odd parity for the OPA-allowed excited states) are maintained for the lower dendrimer generations. However, in higher generations (**S2**, **S3**) a new TPA-allowed state emerges at lower energies ( $\sim 3.25$  eV), which involves a collective excitation from the dendrimer core to the peripheral branches. Moreover, increased torsional disorder in the **S3** molecule leads to breakage of the strict symmetry selection rules, which causes mixing between OPA and TPA states. As a result, the lowest excitations in **S3** become partially

accessible through both linear and two-photon mechanisms. Increased density of the partially TPA-allowed excitations leads to the collective increase in the TPACS in a wide spectral window. However, as the generation grows, the geometry becomes more and more distorted thus preventing further excited-state delocalization. Therefore, the TPA enhancement in **S4** dendrimer is additive rather than cooperative.

### III. Conclusion

In conclusion, excited-state structure underlying linear and two-photon absorption properties of oligothiophene dendrimers proposed for the entangled TPA measurements have been studied experimentally and theoretically. Our combined investigation consistently shows the systematic increase of excitation delocalization with thiophene dendrimer generation, which indicates significant potential of these materials for efficient light-harvesting devices.

We observe several general features of the absorption spectra for the larger dendrimers. Spectral broadening in the red region of absorption spectra have been attributed to the increase of excited-state density with different degrees of excitation delocalization responsible for the bright peaks in the spectra. Conformational distortions in the molecular geometry of larger dendrimers lead to partial mixing of one- and two-photon-allowed excited states and, therefore, to the increase in measured TPA cross sections. Cooperative TPA intensity is observed due to delocalization of excitation in both OPA and TPA processes. To summarize the effect of the dendrimer size on the enhancement of TPACS, there are two factors that are responsible for the growth of TPA intensity in higher generations of thiophene dendrimers: (i) the increase of the excited-state delocalization with the number of thiophene units and (ii) increased density of the TPA-allowed excited states. The first effect saturates at higher generation due to restricted excited-state delocalization as a result of the conformational disorder. The second effect continues to grow with increasing size of the dendrimer and results in an additive increase of the TPACS.

Fluorescence upconversion experiments and TD-DFT calculations of excited-state relaxation reveal the following generation-dependent photoinduced dynamics. Upon excitation, a manifold of moderately delocalized singlet states is reached, which rapidly (within tens of femtoseconds) relaxes to the lowest excited state. The latter is mostly delocalized over the longest quasi-linear  $\alpha$ -thiophene chain, which can be distorted, but nevertheless it preserves  $\pi$ -conjugation supporting delocalization. This is followed by a slow (ps scale) vibronic relaxation involving planarization of this  $\alpha$ -thiophene segment, which then can emit radiatively. Significant generation-dependent Stokes shift is observed, which grows and saturates when the effective exciton length of the emitting chain reaches up to 7–8 thiophene units.

For larger dendrimers, the decrease in the fluorescence quantum yield is explained by an increase in the nonradiative decay rate due to higher probability of intersystem crossing to the triplet states. Such intersystem crossing is more probable in higher dendrimer generations due to increased density of triplet states in the proximity to the lowest singlet excited-state energy region.

**Acknowledgment.** We gratefully acknowledge funding from the Department of Defense, National Science Foundation (TG polymers division), National Geospatial-Intelligence Agency (TG quantum science division), and the German Research Foundation in the frame of Collaborative Research Center 569.

This work was performed in part at the Center for Integrated Nanotechnologies, a U.S. Department of Energy, Office of Basic Energy Sciences user facility. Los Alamos National Laboratory (LANL) is operated by Los Alamos National Security, LLC, for the National Nuclear Security Administration of the U.S. Department of Energy under contract DE-AC52-06NA25396. We acknowledge support of Center for Nonlinear Studies (CNLS) at LANL. E.B. is thankful to the University of Washington Center of Integrated Nanotechnologies UIF fellowship. We also would like to acknowledge funding of the German Science Foundation (DFG) in the frame of Collaborative Research Center SFB 569.

**Supporting Information Available:** Coordinates for the chromophores S1–S3, optimized in a ground state with the HF/6-31G level of theory. This material is available free of charge via the Internet at <http://pubs.acs.org>.

## References and Notes

- Mishra, A.; Ma, C. Q.; Baeuerle, P. *Chem. Rev.* **2009**, *109*, 1141–1276.
- Goodson, T. *Annu. Rev. Phys. Chem.* **2005**, *56*, 581–603.
- Astruc, D.; Boisselier, E.; Ornelas, C. *Chem. Rev.* **2010**, *110*, 1857–1959.
- Goodson, T. *Abstr. Pap. Am. Chem. Soc.* **2004**, *228*, U18–U19.
- Hagedorn, K. V.; Varnavski, O.; Hartwig, J.; Goodson, T. *J. Phys. Chem. C* **2008**, *112*, 2235–2238.
- Varnavski, O.; Baeuerle, P.; Goodson, T. *Opt. Lett.* **2007**, *32*, 3083–3085.
- Bhaskar, A.; Ramakrishna, G.; Hagedorn, K.; Varnavski, O.; Mena-Osteritz, E.; Baeuerle, P.; Goodson, T. *J. Phys. Chem. B* **2007**, *111*, 946–954.
- Varnavski, O.; Goodson, T.; Sukhomlinova, L.; Twieg, R. *J. Phys. Chem. B* **2004**, *108*, 10484–10492.
- Ranasinghe, M. I.; Varnavski, O. P.; Pawlas, J.; Hauck, S. I.; Louie, J.; Hartwig, J. F.; Goodson, T. *J. Am. Chem. Soc.* **2002**, *124*, 6520–6521.
- Varnavski, O. P.; Ostrowski, J. C.; Sukhomlinova, L.; Twieg, R. J.; Bazan, G. C.; Goodson, T. *J. Am. Chem. Soc.* **2002**, *124*, 1736–1743.
- Varnavski, O.; Menkir, G.; Goodson, T.; Burn, P. L. *Appl. Phys. Lett.* **2000**, *77*, 1120–1122.
- Varnavski, O.; Ispasoiu, R. G.; Narewal, M.; Fugaro, J.; Jin, Y.; Pass, H.; Goodson, T. *Macromolecules* **2000**, *33*, 4061–4068.
- Kopelman, R.; Shortreed, M.; Shi, Z. Y.; Tan, W. H.; Xu, Z. F.; Moore, J. S.; BarHaim, A.; Klafter, J. *Phys. Rev. Lett.* **1997**, *78*, 1239–1242.
- BarHaim, A.; Klafter, J.; Kopelman, R. *J. Am. Chem. Soc.* **1997**, *119*, 6197–6198.
- Swallen, S. F.; Shortreed, M. R.; Shi, Z. Y.; Tan, W. H.; Xu, Z. F.; Devadoss, C.; Moore, J. S.; Kopelman, R. *Mol. Cryst. Liq. Cryst. Sci. Technol., Sect. A* **1998**, *314*, 37–46.
- Devadoss, C.; Bharathi, P.; Moore, J. S. *Macromolecules* **1998**, *31*, 8091–8099.
- Devadoss, C.; Bharathi, P.; Moore, J. S. *Angew. Chem., Int. Ed.* **1997**, *36*, 1633–1635.
- Devadoss, C.; Bharathi, P.; Moore, J. S. *J. Am. Chem. Soc.* **1996**, *118*, 9635–9644.
- Adronov, A.; Gilat, S. L.; Frechet, J. M. J.; Ohta, K.; Neuwahl, F. V. R.; Fleming, G. R. *J. Am. Chem. Soc.* **2000**, *122*, 1175–1185.
- Gilat, S. L.; Adronov, A.; Frechet, J. M. J. *Angew. Chem., Int. Ed.* **1999**, *38*, 1422–1427.
- Adronov, A.; Gilat, S. L.; Malenfant, P. R.; Frechet, J. M. J. *Abstr. Pap. Am. Chem. Soc.* **1999**, *217*, U444–U445.
- Andrews, D. L.; Bradshaw, D. S. *J. Chem. Phys.* **2004**, *121*, 2445–2454.
- Balzani, V.; Campagna, S.; Denti, G.; Juris, A.; Serroni, S.; Venturi, M. *Acc. Chem. Res.* **1998**, *31*, 26–34.
- Gust, D.; Moore, T. A.; Moore, A. L. *Acc. Chem. Res.* **2001**, *34*, 40–48.
- Prathapan, S.; Johnson, T. E.; Lindsey, J. S. *J. Am. Chem. Soc.* **1993**, *115*, 7519–7520.
- Cifuentes, M. P.; Powell, C. E.; Morrall, J. P.; McDonagh, A. M.; Lucas, N. T.; Humphrey, M. G.; Samoc, M.; Houbrechts, S.; Asselberghs, I.; Clays, K.; Persoons, A.; Isoshima, T. *J. Am. Chem. Soc.* **2006**, *128*, 10819–10832.
- Hoeben, F. J. M.; Jonkheijm, P.; Meijer, E. W.; Schenning, A. P. H. *J. Chem. Rev.* **2005**, *105*, 1491–1546.
- Katan, C.; Terenziani, F.; Mongin, O.; Werts, M. H. V.; Porres, L.; Pons, T.; Mertz, J.; Tretiak, S.; Blanchard-Desce, M. *J. Phys. Chem. A* **2005**, *109*, 3024–3037.
- Kuzyk, M. G. *J. Chem. Phys.* **2003**, *119*, 8327–8334.
- Macak, P.; Luo, Y.; Norman, P.; Agren, H. *J. Chem. Phys.* **2000**, *113*, 7055–7061.
- Terenziani, F.; Katan, C.; Badaeva, E.; Tretiak, S.; Blanchard-Desce, M. *Adv. Mater.* **2008**, *20*, 4641–4678.
- Varnavski, O.; Yan, X. Z.; Mongin, O.; Blanchard-Desce, M.; Goodson, T. *J. Phys. Chem. C* **2007**, *111*, 149–162.
- Zhou, W. H.; Kuebler, S. M.; Braun, K. L.; Yu, T. Y.; Cammack, J. K.; Ober, C. K.; Perry, J. W.; Marder, S. R. *Science* **2002**, *296*, 1106–1109.
- Larson, D. R.; Zipfel, W. R.; Williams, R. M.; Clark, S. W.; Bruchez, M. P.; Wise, F. W.; Webb, W. W. *Science* **2003**, *300*, 1434–1436.
- He, G. S.; Xu, G. C.; Prasad, P. N.; Reinhardt, B. A.; Bhatt, J. C.; Dillard, A. G. *Opt. Lett.* **1995**, *20*, 435–437.
- Harpham, M. R.; Suzer, O.; Ma, C. Q.; Baeuerle, P.; Goodson, T. *J. Am. Chem. Soc.* **2009**, *131*, 973–979.
- Ramakrishna, G.; Bhaskar, A.; Baeuerle, P.; Goodson, T. *J. Phys. Chem. A* **2008**, *112*, 2018–2026.
- Kaino, T. *J. Opt. A: Pure Appl. Opt.* **2000**, *2*, R1–R7.
- Ledoux, I.; Zyss, J. *Int. J. Nonlinear Opt. Phys.* **1994**, *3*, 287–316.
- Tatsuura, S.; Matsubara, T.; Tian, M. Q.; Mitsu, H.; Iwasa, I.; Sato, Y.; Furuki, M. *Appl. Phys. Lett.* **2004**, *85*, 540–542.
- Tretiak, S.; Middleton, C.; Chernyak, V.; Mukamel, S. *J. Phys. Chem. B* **2000**, *104*, 4519–4528.
- Minami, T.; Tretiak, S.; Chernyak, V.; Mukamel, S. *J. Lumin.* **2000**, *87*–*9*, 115–118.
- Wu, C.; Malinin, S. V.; Tretiak, S.; Chernyak, V. Y. *J. Chem. Phys.* **2008**, *129*, 174113(1–7).
- Wu, C.; Malinin, S. V.; Tretiak, S.; Chernyak, V. Y. *Phys. Rev. Lett.* **2008**, *100*, 057405–057409.
- Zade, S. S.; Bendikov, M. *J. Org. Chem.* **2006**, *71*, 2972–2981.
- Fichou, D. *J. Mater. Chem.* **2000**, *10*, 571–588.
- Perepichka, I. F.; Perepichka, D. F.; Meng, H.; Wudl, F. *Adv. Mater.* **2005**, *17*, 2281–2305.
- Garnier, F.; Hajlaoui, R.; Yassar, A.; Srivastava, P. *Science* **1994**, *265*, 1684–1686.
- Ong, B. S.; Wu, Y. L.; Liu, P.; Gardner, S. *J. Am. Chem. Soc.* **2004**, *126*, 3378–3379.
- Holliday, B. J.; Swager, T. M. *Chem. Commun.* **2005**, 23–36.
- Chen, T. A.; Rieke, R. D. *J. Am. Chem. Soc.* **1992**, *114*, 10087–10088.
- Lanzani, G.; Nisolli, M.; DeSilvestri, S.; Barbarella, G.; Zambianchi, M.; Tubino, R. *Phys. Rev. B* **1996**, *53*, 4453–4457.
- Lanzani, G.; Nisolli, M.; DeSilvestri, S.; Tubino, R. *Chem. Phys. Lett.* **1996**, *251*, 339–345.
- Lanzani, G.; Nisolli, M.; DeSilvestri, S.; Tubino, R. *Synth. Met.* **1996**, *76*, 39–41.
- Westenhoff, S.; Beenken, W. J. D.; Friend, R. H.; Greenham, N. C.; Yartsev, A.; Sundstrom, V. *Phys. Rev. Lett.* **2006**, *97*, 166804–166808.
- Ma, C. Q.; Mena-Osteritz, E.; Debaerdemaecker, T.; Wienk, M. M.; Janssen, R. A. J.; Baeuerle, P. *Angew. Chem., Int. Ed.* **2007**, *46*, 1679–1683.
- Grebner, D.; Helbig, M.; Rentsch, S. *J. Phys. Chem.* **1995**, *99*, 16991–16998.
- Kodaira, T.; Watanabe, A.; Ito, O.; Watanabe, M.; Saito, H.; Koishi, M. *J. Phys. Chem.* **1996**, *100*, 15309–15313.
- Cheng, X.; Ichimura, K.; Fichou, D.; Kobayashi, T. *Chem. Phys. Lett.* **1991**, *185*, 286–291.
- Westenhoff, S.; Daniel, C.; Friend, R. H.; Silva, C.; Sundstrom, V.; Yartsev, A. *J. Chem. Phys.* **2005**, *122*, 094903–094911.
- Yang, A.; Kuroda, M.; Shiraishi, Y.; Kobayashi, T. *J. Phys. Chem. B* **1998**, *102*, 3706–3711.
- Fujitsuka, M.; Cho, D. W.; Ohshita, J.; Kunai, A.; Majima, T. *J. Phys. Chem. B* **2006**, *110*, 12446–12450.
- Fujitsuka, M.; Cho, D. W.; Ohshita, J.; Kunai, A.; Majima, T. *J. Phys. Chem. C* **2007**, *111*, 1993–1998.
- Varnavski, O.; Samuel, I. D. W.; Palsson, L. O.; Beavington, R.; Burn, P. L.; Goodson, T. *J. Chem. Phys.* **2002**, *116*, 8893–8903.
- Runge, E.; Gross, E. K. U. *Phys. Rev. Lett.* **1984**, *52*, 997–1000.
- Casida, M. E. In *Recent Advances in Density-Functional Theory Methods*; Chong, D. A., Ed.; World Scientific: Singapore, 1995; Vol. 3.
- Jamorski, C.; Casida, M. E.; Salahub, D. R. *J. Chem. Phys.* **1996**, *104*, 5134–5147.
- Furche, F.; Ahlrichs, R. *J. Chem. Phys.* **2002**, *117*, 7433–7447.
- Oudar, J. L. *J. Chem. Phys.* **1977**, *67*, 446–457.
- Berman, O.; Mukamel, S. *Phys. Rev. B* **2003**, *68*, 104519–104528.
- Tretiak, S.; Chernyak, V. *J. Chem. Phys.* **2003**, *119*, 8809–8823.
- Masunov, A. M.; Tretiak, S. *J. Phys. Chem. B* **2004**, *108*, 899–907.

- (73) Kobko, N.; Masunov, A.; Tretiak, S. *Chem. Phys. Lett.* **2004**, *392*, 444–451.
- (74) Bartholomew, G. P.; Rumi, M.; Pond, S. J. K.; Perry, J. W.; Tretiak, S.; Bazan, G. C. *J. Am. Chem. Soc.* **2004**, *126*, 11529–11542.
- (75) Badaeva, E. A.; Timofeeva, T. V.; Masunov, A. M.; Tretiak, S. *J. Phys. Chem. A* **2005**, *109*, 7276–7284.
- (76) Kauffman, J. F.; Turner, J. M.; Alabugin, I. V.; Breiner, B.; Kovalenko, S. V.; Badaeva, E. A.; Masunov, A.; Tretiak, S. *J. Phys. Chem. A* **2006**, *110*, 241–251.
- (77) Katan, C.; Tretiak, S.; Werts, M. H. V.; Bain, A. J.; Marsh, R. J.; Leonczek, N.; Nicolaou, N.; Badaeva, E.; Mongin, O.; Blanchard-Desce, M. *J. Phys. Chem. B* **2007**, *111*, 9468–9483.
- (78) Tretiak, S.; Mukamel, S. *Chem. Rev.* **2002**, *102*, 3171–3212.
- (79) Frisch, M. J.; Trucks, G. W.; Schlegel, H. B.; Scuseria, G. E.; Robb, M. A.; Cheeseman, J. R.; Montgomery, J. A., Jr.; Vreven, T.; Kudin, K. N.; Burant, J. C.; Millam, J. M.; Iyengar, S. S.; Tomasi, J.; Barone, V.; Mennucci, B.; Cossi, M.; Scalmani, G.; Rega, N.; Petersson, G. A.; Nakatsuji, H.; Hada, M.; Ehara, M.; Toyota, K.; Fukuda, R.; Hasegawa, J.; Ishida, M.; Nakajima, T.; Honda, Y.; Kitao, O.; Nakai, H.; Klene, M.; Li, X.; Knox, J. E.; Hratchian, H. P.; Cross, J. B.; Bakken, V.; Adamo, C.; Jaramillo, J.; Gomperts, R.; Stratmann, R. E.; Yazyev, O.; Austin, A. J.; Cammi, R.; Pomelli, C.; Ochterski, J. W.; Ayala, P. Y.; Morokuma, K.; Voth, G. A.; Salvador, P.; Dannenberg, J. J.; Zakrzewski, V. G.; Dapprich, S.; Daniels, A. D.; Strain, M. C.; Farkas, O.; Malick, D. K.; Rabuck, A. D.; Raghavachari, K.; Foresman, J. B.; Ortiz, J. V.; Cui, Q.; Baboul, A. G.; Clifford, S.; Cioslowski, J.; Stefanov, B. B.; Liu, G.; Liashenko, A.; Piskorz, P.; Komaromi, I.; Martin, R. L.; Fox, D. J.; Keith, T.; Al-Laham, M. A.; Peng, C. Y.; Nanayakkara, A.; Challacombe, M.; Gill, P. M. W.; Johnson, B.; Chen, W.; Wong, M. W.; Gonzalez, C.; Pople, J. A. *Gaussian 03*, revision D.01; Gaussian, Inc.: Wallingford, CT, 2004.
- (80) Magyar, R. J.; Tretiak, S. *J. Chem. Theory Comput.* **2007**, *3*, 976–987.
- (81) Martin, R. L. *J. Chem. Phys.* **2003**, *118*, 4775–4777.
- (82) Zhao, M. T.; Singh, B. P.; Prasad, P. N. *J. Chem. Phys.* **1988**, *89*, 5535–5541.
- (83) Ramakrishna, G.; Goodson, T. *J. Phys. Chem. A* **2007**, *111*, 993–1000.
- (84) Rentsch, S.; Yang, J. P.; Paa, W.; Birckner, E.; Schiedt, J.; Weinkauf, R. *Phys. Chem. Chem. Phys.* **1999**, *1*, 1707–1714.
- (85) Paa, W.; Yang, J. P.; Helbig, M.; Hein, J.; Rentsch, S. *Chem. Phys. Lett.* **1998**, *292*, 607–614.
- (86) Paa, W.; Yang, J. P.; Rentsch, S. *Appl. Phys. B* **2000**, *71*, 443–449.
- (87) Nakano, M.; Fujita, H.; Takahata, M.; Yamaguchi, K. *J. Am. Chem. Soc.* **2002**, *124*, 9648–9655.

JP109624D